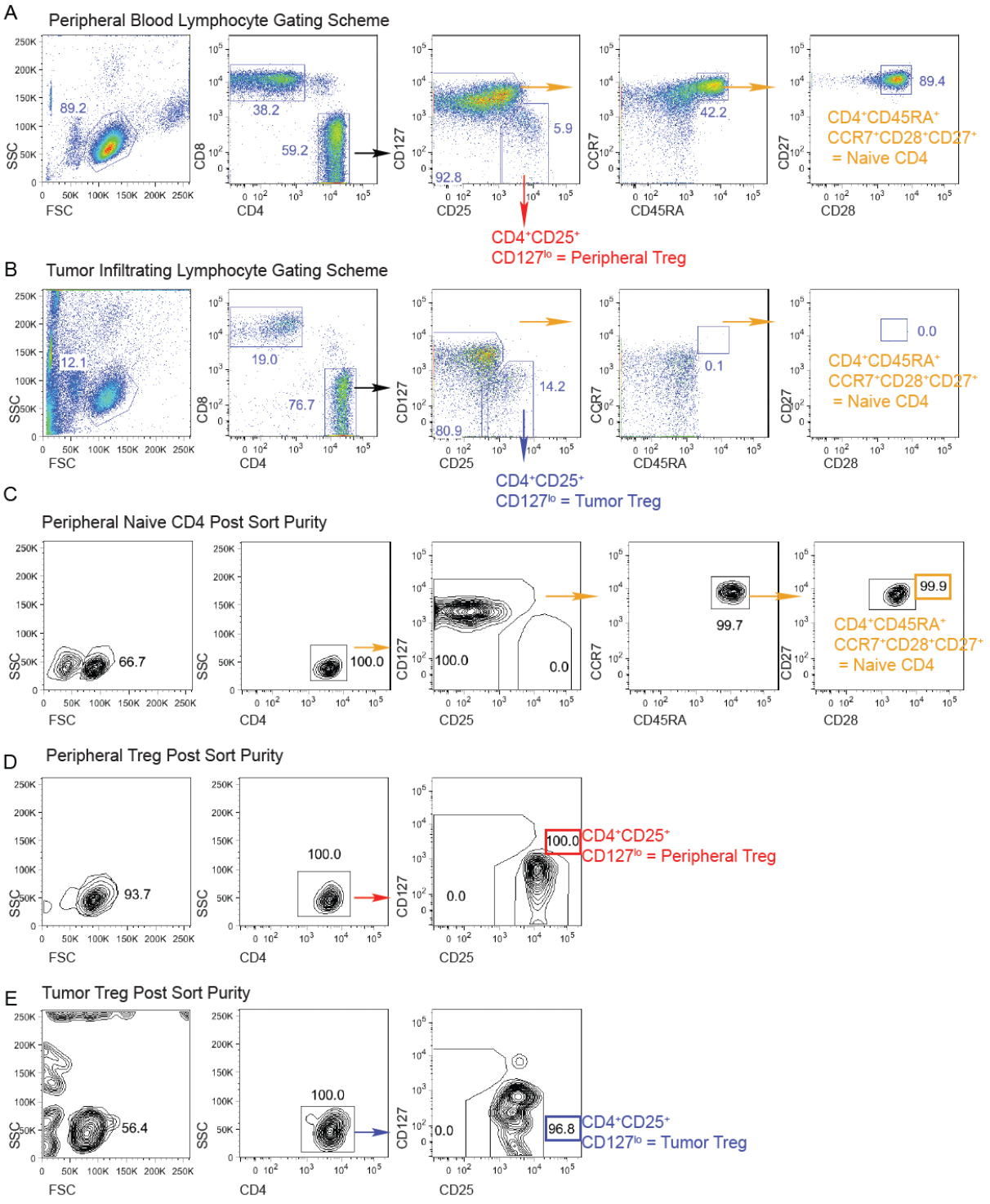

Figure S1 Human T Cell Sorting Schemes and Purity, related to Figure 1: (A) Sorting scheme for flow isolation of peripheral blood $CD8^+$ T cells and Tregs. **(B)** Sorting scheme for flow isolation of tumor infiltrating CD8, Treg, and naïve CD4 Tconv populations. **(C)** Purity of

peripheral blood naïve CD4 T cells post-sort. **(D)** Purity of peripheral blood Tregs post-sort. **E)** Purity of TI-Tregs post-sort.

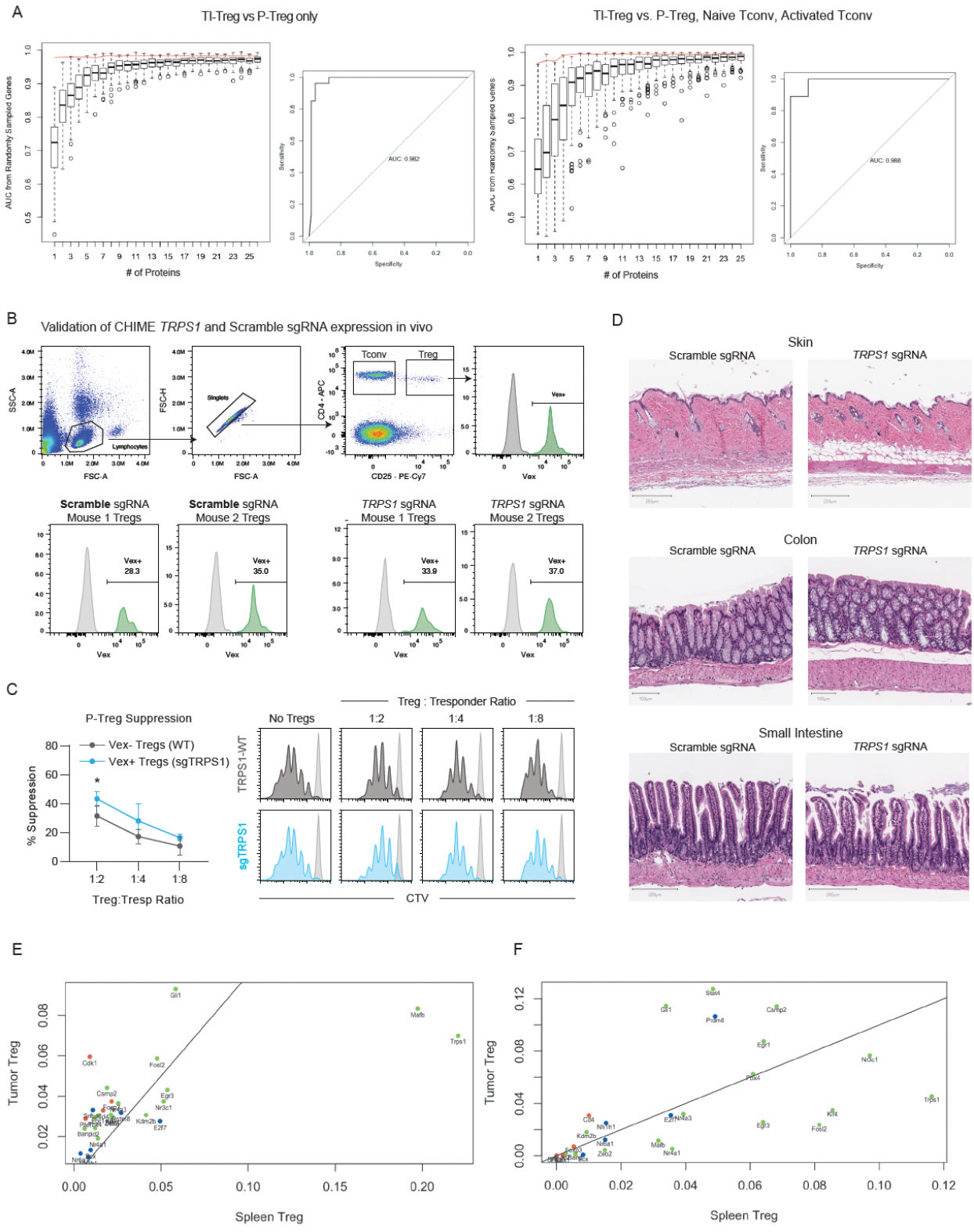

Figure S2: CRISPR KO Transduction Efficiency and Individual Cohort Results, related to Figures 1 and 2: (A) Random Forest Feature Selection of VIPER Master Regulators. Boxplots

show distribution of test-AUCs for randomly sampled number of genes corresponding to x-axis, with red line indicating actual AUC of the Master Regulator gene set. AUC of master regulator gene set for the selected number of MRs is shown in inset to the right. Left plots show feature selection of TI-Treg vs P-Treg MRs, right plots show the same for TI-Treg vs combined set of non-TI-Treg controls. **(B)** Flow gating schema and sgRNA transduction efficiency following immune reconstitution of CHIME animals. Vex+ frequencies of peripheral blood Treg populations are shown for two representative mice per condition. **(C)** Treg suppression assay performed with Trps1-sgRNA Vex+ Tregs (blue) versus Vex- wild-type Tregs (grey), showing no statistically significant difference in % T-cell suppression at all tested Treg to Tresponder ratios. **(D)** H&E stained slides of peripheral tissues (Skin, Colon, Small intestine) from Scramble-sgRNAs control mice (left) versus Trps1-sgRNA mice (right). All tissues showing no signs of autoimmunity per review by trained pathologist. **(E)** Frequency scatterplot of sgRNAs targeting each gene in Tumor Tregs versus Spleen Tregs from CRISPR screen described in Figure 2. Frequencies shown are for Experimental cohort 1, with green dots showing candidate MRs, red dots showing positive control genes, blue dots showing negative control genes, and solid black line at equal frequency in Tumor vs Spleen. **(F)** Frequency scatterplot as in E, showing sgRNA frequencies in Experimental cohort 2.

A

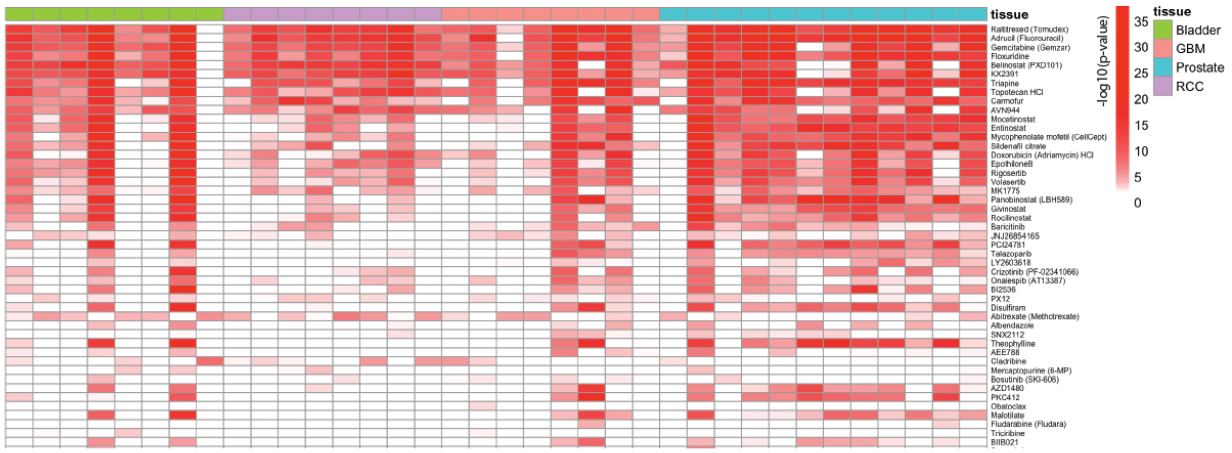

B

Drug	-log10(Bonferroni-Corrected p-value)	Concentration
Raltitrexed (Tomudex)	16.0120428	10uM
Gemcitabine (Gemzar)	14.0907063	0.01uM
Adrucil (Fluorouracil)	13.8004313	9uM
Floxuridine	13.0250749	0.5uM
Triapine	12.5682276	1.5uM
KX2391	12.4838562	0.5uM
Topotecan HCl	12.3860404	0.065uM
Volasertib	11.1958988	0.24uM
EpothiloneB	9.67898425	8.5uM
Doxorubicin (Adriamycin) HCl	9.47823228	0.16uM
Mycophenolate mofetil	8.5938642	10uM
Belinostat (PXD101)	7.07684924	0.14uM
Rigosertib	7.05275929	0.08uM
Panobinostat (LBH589)	6.93053883	0.07uM
Sildenafil citrate	6.49302924	2uM
Carmofur	5.82534374	1uM
Theophylline	5.52492604	10uM
Onalespib (AT13387)	5.23334434	0.035uM
Talazoparib	5.05827958	0.5uM
Entinostat	4.62376284	1uM
PCI24781	4.61786217	0.2uM
PKC412	4.51702539	0.07uM
AVN944	4.23345055	0.215uM
Mocetinostat	3.62168835	0.5uM
Vorinostat (SAHA; MK0683)	3.4288806	2.5uM
BI2536	3.24077657	1uM
Rocilinostat	2.89525071	1uM
Pralatrexate(Folotyn)	2.79171615	0.2uM
Givinostat	2.437055	0.16uM
17-AAG (Tanespimycin)	2.39042227	0.085uM
MK1775	2.27975304	0.13uM
Malotilate	1.75540515	1.5uM

Figure S3: Tumor-Treg OncoTreat Drug Predictions, Expanded List of All Statistically Significant Compounds, related to Figure 3: (A) Patient-by-Patient Drug predictions

according to inversion of patient-specific Tumor Treg vs Peripheral Treg protein activity signature by drug-treatment protein activity signature. Each drug predicted to invert Tumor Treg signature with -log10(Bonferroni-Corrected p-value) < 0.01 in a particular patient is colored red. Patients are grouped by tumor type. **(B)** Table of all drugs significantly down-regulating Tumor-Treg MRs identified in Figure 1E, 1F, ordered by p-value. Drugs also identified by growth screen to have differentially higher toxicity in Tumor Tregs vs Peripheral Tregs are highlighted in yellow. All seven of these are identified as statistically significant hits down-regulating Tumor-Treg MRs.

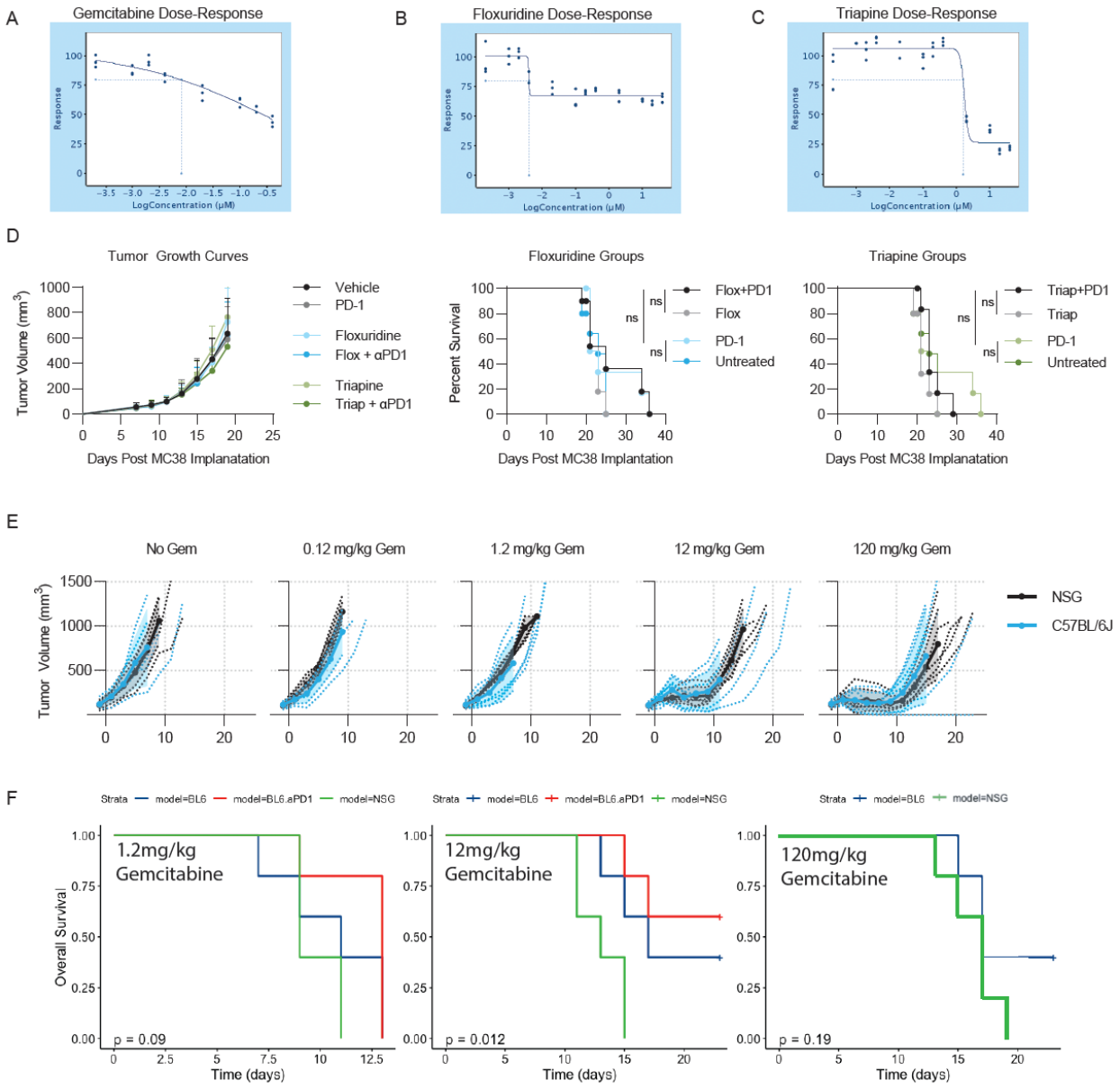

Figure S4: In-vivo Tumor Growth Inhibition by Gemcitabine, Floxuridine, and Triapine, related to Figures 3 and 4: (A) Dose-response titration curve for gemcitabine on ex vivo Treg growth inhibition. **(B)** Dose-response titration curve for floxuridine on ex vivo Treg growth inhibition. **(C)** Dose-response titration curve for triapine on ex vivo Treg growth inhibition. **(D)** Tumor growth curves over time for each treatment (vehicle, floxuridine, triapine, anti-PD-1, anti-PD-1+floxuridine, anti-PD-1+triapine), data shown as mean across mice, Kaplan-Meier curves

for floxuridine treatment groups and triapine treatment groups. **(E)** Tumor growth curves of gemcitabine titration at 120 mg/kg, 12 mg/kg, 1.2 mg/kg, and 0.12 mg/kg doses in NSG vs C57BL/6J mice. **(F)** Kaplan-Meier curves of gemcitabine dose titration at 1.2mg/kg, 12mg/kg, and 120mg/kg, showing comparison of overall survival time in BL6 immune-competent mice (with or without aPD1) versus NSG immunodeficient mice ($p = 0.09$, $p = 0.012$, and $p = 0.19$, respectively)

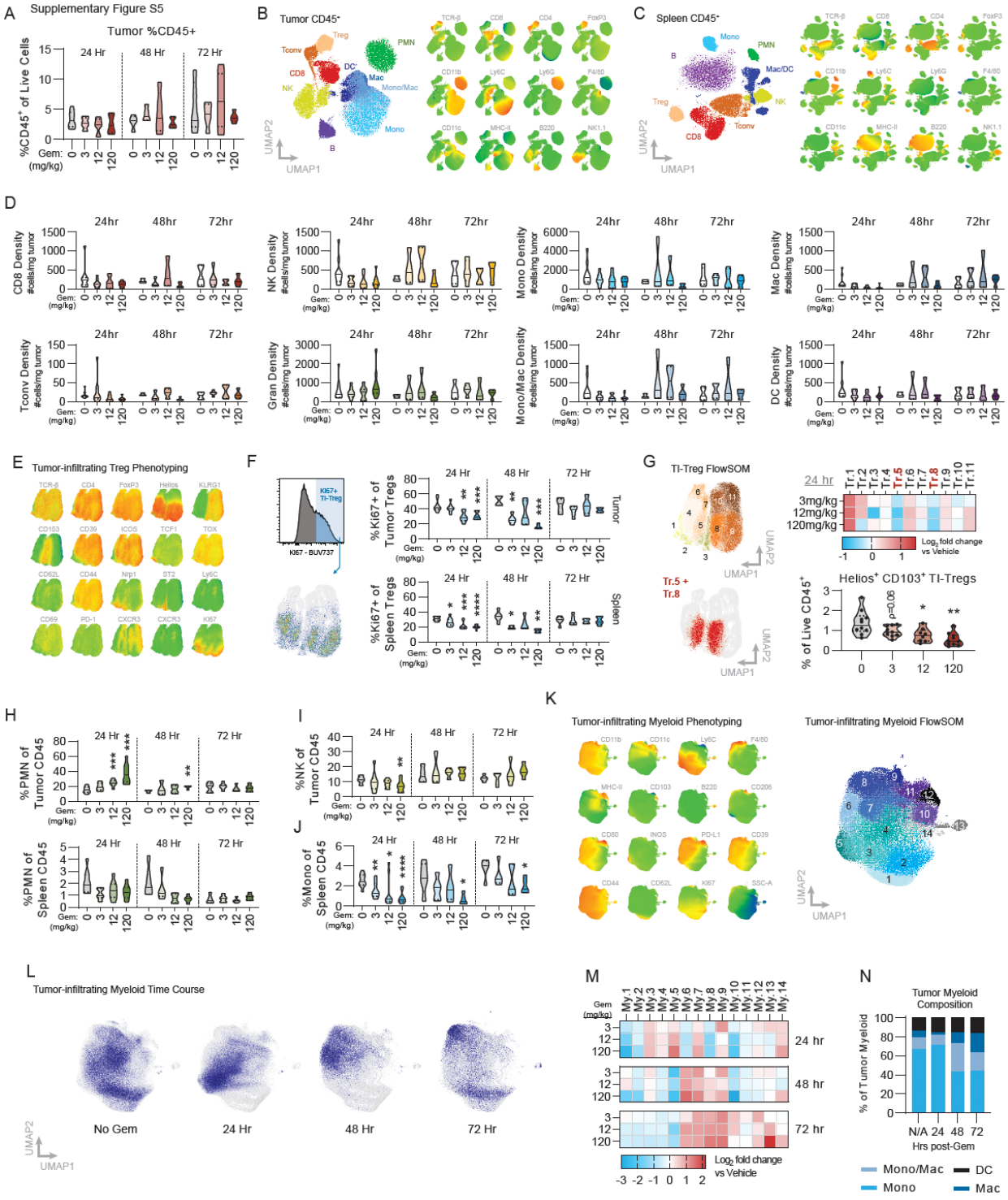

Figure S5: Flow Cytometry Characterization of Immune Repertoire in Gemcitabine-Treated MC38 Tumors, related to Figure 4: (A) Overall CD45+ immune cell frequencies in tumors, grouped by timepoint and gemcitabine dose. **(B)** Overall flow cytometry clustering of

tumor immune cells, with heatplots showing expression of lineage marker proteins by cluster. **(C)** Overall flow cytometry clustering of spleen immune cells, with heatplots showing expression of lineage marker proteins by cluster. **(D)** Violin plots of immune cell densities grouped by timepoint and gemcitabine dose. No populations are statistically significantly changed by two-way ANOVA with multiple comparisons correction. **(E)** UMAP plot of Tregs only, with heatplots showing expression of 20 phenotypic markers. **(F)** Distribution of KI67 showing KI67+ Tregs and their frequency in Tumor and Spleen, grouped by timepoint and gemcitabine dose. **(G)** Unsupervised sub-clustering of Tregs by flow cytometry markers, with heatmap showing log-fold-change versus vehicle for each cluster at 24 hours of gemcitabine treatment and violinplot of Helios+CD103+ Treg frequencies, representing combination of unsupervised clusters Tr.5 and Tr.8. **(H)** Polymorphonuclear cell (PMN) frequencies in tumor and spleen, grouped by timepoint and gemcitabine dose. **(I)** NK cell frequencies in tumor, grouped by timepoint and gemcitabine dose. **(J)** Monocyte frequencies in spleen, grouped by timepoint and gemcitabine dose. **(K)** UMAP plot of monocytes only, with heatplots showing expression of 16 phenotypic markers, unsupervised clustering of monocytes by flow cytometry shown to the right. **(L)** Distribution of monocytes shown split by gemcitabine treatment timepoint. **(M)** Heatmap showing log-fold-change versus vehicle for each monocyte cluster at 24, 48, and 72 hours of gemcitabine treatment. **(N)** Stacked barplot of major myeloid population frequencies at 120mg/kg of gemcitabine, grouped by treatment timepoint, showing relative decrease in undifferentiated monocytes and increase in more mature monocyte/macrophages and terminally differentiated macrophages.

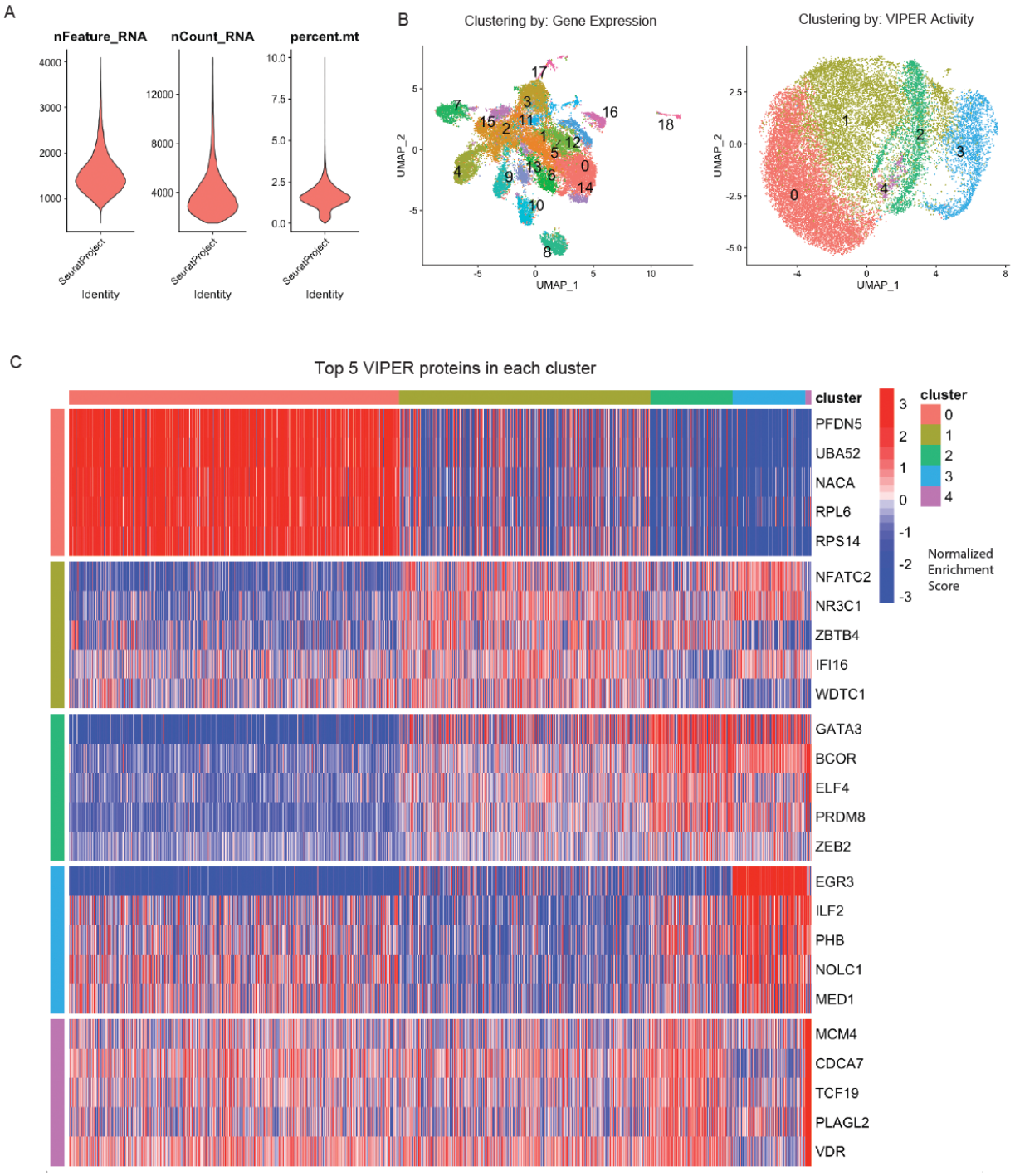

Figure S6: **Single-Cell RNA-Seq Characterization of Tumor-Infiltrating and Peripheral Tregs With or Without Low-Dose Gemcitabine Treatment, related to Figure 5: (A)** Violin plot of data quality showing distribution of nFeature_RNA (number of unique genes profiled), nCount_RNA (number of unique molecular identifiers profiled), and percent.mt (percentage of

mitochondrial transcripts) per cell. **(B)** Clustering of Tregs by Gene Expression (left) and VIPER protein activity inference (right), showing noisiness of clustering by gene expression due to cross-sample batch effects. **(C)** Top5 most differentially upregulated proteins per Treg cluster.